applied sciences

MDPI

Article

A Multilevel Adaptive Path-Planning Model in Off-Road Environments

Xiaobo Song and Jingwei Gao *

College of Aerospace Science and Engineering, National University of Defense Technology, Changsha 410015, China
* Correspondence: gaojingwei@nudt.edu.cn

Abstract: Most existing path-planning algorithms are applied in either trafficable environments or non-trafficable environments. Off-road vehicles (ORVs) are often faced with a mix of trafficable and non-trafficable environments. Therefore, trafficability should be considered in path planning for ORVs. Conventional ant colony algorithms (ACAs) are prone to stagnation and often fail to reach the optimal path. To address these problems, an improved ACA that considers trafficability was proposed in this study, which improved the pheromone distribution rules and adaptively adjusted the pheromone volatility coefficient. Based on this improved ACA, a multilevel adaptive path-planning model was proposed to solve path-planning problems with various scales of area. Experiments and comparative studies revealed that the improved ACA was applicable to path-planning problems in complex environments and achieved better performance and a higher computing efficiency than conventional counterparts.

Keywords: ant colony algorithm; path planning; trafficability; multilevel adaptability

check for updates

Citation: Song, X.; Gao, J. A Multilevel Adaptive Path-Planning Model in Off-Road Environments. *Appl. Sci.* **2022**, *12*, 10706. https://doi.org/10.3390/app122110706

Academic Editor: Vincent A. Cicirello

Received: 20 September 2022
Accepted: 13 October 2022
Published: 22 October 2022

Publisher's Note: MDPI stays neutral with regard to jurisdictional claims in published maps and institutional affiliations.

Copyright: © 2022 by the authors. Licensee MDPI, Basel, Switzerland. This article is an open access article distributed under the terms and conditions of the Creative Commons Attribution (CC BY) license (https://creativecommons.org/licenses/by/4.0/).

1. Introduction

Existing path-planning algorithms are applicable only to specific scenarios, such as container transport at ports [1,2], warehouse logistics [3,4], and obstacle avoidance in robots [5–7]. When applied to engineering fields such as agricultural machinery, forest fire protection, traffic, and transportation, the algorithm needs to be designed to find the optimal trafficable path by considering the possibility that there might be no road or only rugged roads amid hills and mountains. The environments for these scenarios are more complex and the path length can range from several to hundreds of kilometers. Therefore, it is crucial to find a path-planning model for long-distance off-road environments.

The first step of path planning is to process the real-world environment and construct an environmental model. The grid map method, topological method, and Voronoi diagram method are common modeling methods. The grid map method converts the area to be studied into cells, which are termed grids. In recent years, many types of grids have been proposed including diamond grids, fan grids, and honeycomb grids [8–10], but the most intensively studied is the rectangular grid. The different trafficability properties of the grids indicate whether the regions they represent are trafficable or not.

Popular path-planning algorithms include traditional algorithms such as the Dijkstra algorithm and the rapidly exploring random tree (RRT) algorithm, as well as intelligent algorithms such as the genetic algorithm and ant colony algorithm. The traditional algorithms, which were proposed earlier and are based on simple mechanics, have been widely used, especially in path planning for unmanned aerial vehicles (UAVs) [11,12] and driverless cars [13,14]. The fundamental algorithms represented by reactive path-planning algorithms [15–18] such as potential field, velocity obstacle, collision cone, etc., also play a huge role in solving such problems. Karmokar et al. [15] presented a novel vision-based framework for tracking dynamic objects using guidance laws based on a rendezvous cone approach. Furthermore, by performing a series of simulations to show the efficacy of

their methods, Dhal et al. [16] modelled the shapes of objects using quadric surfaces. A collision/rendezvous cone concept was employed. A computationally efficient approach was presented to compute the collision/rendezvous cone between finite-sized quadric surfaces (which were not necessarily of the same shape).

As bionics research advances and interdisciplinary studies develop, intelligent algorithms are seeing wider adoption in path planning. In 1992, Dorigo et al. [19] put forward the ant colony algorithm (ACA). Inspired by foraging behaviors of ants that often find the shortest path towards food, ACA has gained popularity in path-planning tasks. Ezhilarasi [20] proposed an algorithm using fuzzy ant clustering, which detected and combined the overlapping nodes to reduce the redundancy and improve the quality of the clusters. To address the intrinsic susceptibility of ACAs to a local optimum, Ning [21] adjusted the initial distribution of pheromones by introducing new heuristic functions and adaptive updating rules of pheromones.

Many solutions have been proposed for off-road path planning. To find the optimal path for off-road autonomous driving with static obstacle avoidance, Chu et al. [22] determined the priority of each path by considering the path safety cost, path smoothness, and path consistency. Chen et al. [23] proposed a path-planning method based on fuzzy support vector machine (FSVM) and general regression neural network (GRNN) to provide a solution path for autonomous vehicles navigating in off-road environments and verified through experiments that their method could navigate vehicles on smooth and obstacle-free routes when satisfying the constraint of vehicle kinematics. Wang et al. [24] considered the influence of terrain slope and soil strength on a vehicle's off-road trafficability. A tabu table and grid-weight table were used in their study to determine the trafficability of off-road regions. Simulations based on a tracked vehicle M1A1 in off-road environments showed that their improved ant colony path-planning algorithm considerably improved computation efficiency. In correspondence to two kinds of obstacles and terrains in the path planning of unmanned tracked vehicles, Hu et al. [25] introduced different types of potential energy function models and designed a multi-stage optimization channel path-planning method with the potential field gradient as a condition of optimization. Ji et al. [26], based on 3D terrain map information, employed a random-sampling-based scheme so that vehicles can adaptively generate a path in complex environments within a short time. To address the problem of unknown environments in local path planning, Yang et al. [27] proposed a target point extraction algorithm to extract targets in free spaces and found in their experiments that their method performed well in long-distance path planning. Jiang et al. [28] defined two metrics for the path planning of off-road autonomous ground vehicles under uncertain terrain environments, namely state mobility reliability and mission mobility reliability. They also developed a path-smoothing algorithm to address the suboptimality of their method. Goodin et al. [29] accounted for LIDAR–vegetation interaction and developed a LIDAR processing algorithm for off-road autonomous navigation, which can distinguish navigable vegetation from non-navigable solid obstacles and has practical value for the development of autonomous off-road navigation algorithms. To address the limited capacity of conventional methods in long-distance off-road path planning, Hong et al. [30] put forward an improved A-Star algorithm based on terrain data; their improved method achieved a path-planning efficiency 4.6 times higher and a maximum acceleration 550 times higher than the conventional A-Star algorithm.

Based on previous works on off-road path planning, a multilevel adaptive path-planning model based on improved ACA was proposed in the present study. The influence of terrain and surface features on road trafficability was used as the key information to adjust the algorithm to fit areas of different scales so that the model could be effectively applied to large areas and complex environments.

2. Overview of Ant Colony Algorithm and Improvements

2.1. Basic Mathematical Model for the Ant Colony Algorithm

An ant colony algorithm (ACA) is an abstract expression of the foraging behaviors of ants in the natural world. In an ACA, the path pheromone concentration between nodes decides the motion of ants. An ant at a given node i calculates the probability to move towards the next optional node, and if an ant k moves from node i to another node j at the time t, then its motion transfer probability is expressed as follows:

$$P_{i,j}^{k}(t) = \begin{cases} \frac{\tau_{i,j}^{\alpha}(t)\cdot\eta_{i,j}^{\beta}(t)}{\sum_{j\in allowed\_k}\tau_{i,j}^{\alpha}(t)\cdot\eta_{i,j}^{\beta}(t)}, j \in A_k \\ 0, else \end{cases} \quad (1)$$

where A_k is the set of selectable nodes that the ant k can move to at the next time point; $\eta_{i,j}(t)$ is the expectation heuristic function, which represents the expectation value that the ant moves from i to j. $\eta_{i,j}(t)$ can be calculated by Equation (2), where E is the location of the target point and $d(i, E)$ is the distance between node i and target node:

$$\eta_{i,j}(t) = \frac{1}{d(i,E)} \quad (2)$$

$\tau_{i,j}(t)$ is the pheromone concentration on the route from node i to node j at the time point t. After each round of global updating, the pheromone concentration of the route will be updated by a given strategy, and the update equation is as follows:

$$\tau_{i,j}(t+n) = (1-\rho)\cdot\tau_{i,j}(t) + \Delta\tau_{i,j} \quad (3)$$

where $1-\rho$ is the residual coefficient of pheromone, and a larger value of $1-\rho$ indicates less volatility of the pheromone; $\Delta\tau_{i,j}$ represents the increment of pheromone along the $i-j$ route during iteration, which is expressed as follows:

$$\Delta\tau_{i,j} = \sum_{k=1}^{m}\Delta\tau_{i,j}^{k} \quad (4)$$

where $\Delta\tau^{k}{}_{i,j}$ is the pheromone that the ant k releases along the $i-j$ route during iteration. The calculation methods vary as the pheromone update rules differ. The ant cycle system is the most popular update rule, which updates the pheromone after a feasible solution is found after iteration. $\Delta\tau^{k}{}_{i,j}$ is calculated by Equation (5):

$$\Delta\tau_{i,j}^{k} = \begin{cases} \frac{Q}{L_k}, \text{when ant } k \text{ passes through route } i\text{–}j \\ 0, \text{else} \end{cases} \quad (5)$$

where Q is the pheromone concentration and L_k is the length of the route that the ant k moves during the iteration.

2.2. Improvements on ACA

2.2.1. Improved State Transition Probability Equation

The driving cycle of off-road vehicles are not on paved roads, but a complex environment with grassland, bare land, mire, etc., and the traveling time of vehicles varies on different surfaces. Therefore, in path planning, it is necessary to consider heuristic information in terms of trafficability to improve the state transition probability equation. Equation (6) shows the improved state transition probability equation:

$$P_{i,j}^{k}(t) = \begin{cases} \frac{\tau_{i,j}^{\alpha}(t)\cdot\eta_{i,j}^{\beta}(t)\cdot p_{i,j}^{\gamma}(t)}{\sum_{j\in allowed\_k}\tau_{i,j}^{\alpha}(t)\cdot\eta_{i,j}^{\beta}(t)\cdot p_{i,j}^{\gamma}(t)}, j \in A_k \\ 0, else \end{cases} \quad (6)$$

where $p_{i,j}$ is the trafficability heuristic information function.

Figure 1 interprets the difference between the original algorithm and the improved one. The ant can move from the start point S to the current grid in seven possible directions, as shown in Figure 1a. When only the impact of expectation heuristic information on the ant's decision is considered, the ant is likely to move to a grid closer to the destination E, as shown in Figure 1b. Figure 1c shows the possible moving directions when the heuristic information is considered, which suggests that the heuristic information plays a guiding role in an ant's decision-making. In the improved ACA, both the expectation heuristic information and trafficability heuristic information are included in the state transition probability equation; in this case, the ant will move to a grid with better expectation and better trafficability, as shown in Figure 1d.

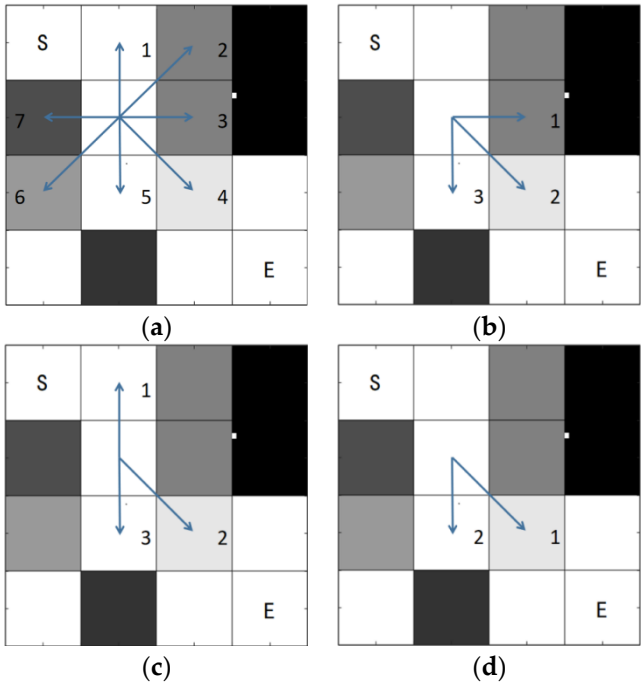

Figure 1. Diagrams of moving directions. (**a**) Seven transferable directions. (**b**) Excellent transferable direction when only expectation heuristic information is considered. (**c**) Excellent transferable direction when only passing heuristic information is considered. (**d**) Excellent transferable direction when heuristic information is comprehensively considered.

2.2.2. Improved Pheromone Update Model

Pheromone distribution follows the rule of even distribution, that is, the pheromone on each segment of the shortest route is evenly distributed. In the foraging process, however, the probability that an ant chooses each segment differs. Figure 2 shows three different routes followed by three ants from grid 1 to grid 16, which are 1–6–11–16, 1–5–6–11–16, and 1–2–3–7–11–16, respectively. Obviously, the route 11–16 has the largest weight in the ants' decision-making. Therefore, it is necessary to improve the original pheromone update model to distribute more pheromone to routes with a higher probability of being chosen.

The pheromone increment calculation equation is improved to achieve a better convergence performance, to strengthen the role of frequent routes in ants' decision-making, and to preclude the problem of the local optimum, as shown in Equation (7):

$$\Delta\tau_{i,j}^{k} = \begin{cases} \mu_{i,j}\frac{Q}{L_k}, \text{when ant } k \text{ passes through route } i\text{–}j \\ 0, \text{else} \end{cases} \quad (7)$$

where $\mu_{i,j}$ is the weight coefficient for the route from grid i to grid j.

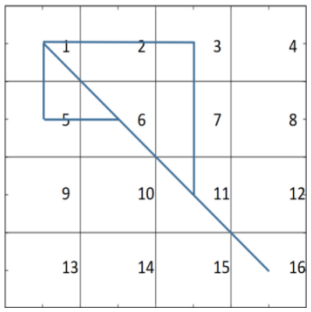

Figure 2. Moving routes of ants.

The Softplus activation function is used to define the value of $\mu_{i,j}$, which is expressed as $f(x) = \log_2[1 + e^x]$; the value of x is in the range [0, 1]; and the value of the function is within the range $[1, \log_2(1 + e)]$, which monotonously increases in the domain of definition. In this function, x is defined as follows:

$$x = \frac{M_{i,j} - M_{\min}}{M_{\max} - M_{\min}} \tag{8}$$

where $M_{i,j}$ is the number of times that the ant chooses the route $I - j$ during iterations, $M_{\max}$ represents the maximum number of times that the ant chooses each route during iterations, and $M_{\min}$ represents the minimum number of times that the ant chooses each route during iterations.

2.2.3. Adaptive ACA

To address the problem of stagnation that conventional ACAs are susceptible to, we introduce an adaptive ACA. Compared with conventional ACAs, the adaptive ACA shows the following improvements:

(1) Introducing the pheromone-smoothing mechanism to improve the algorithm's performance.

In conventional ACAs, the pheromone volatility coefficient is a constant. In the initial stage of algorithm implementation, to avoid the excessive impacts of positive feedback on the ant colony and the risk of a local optimum, the value of ρ should be kept to a minimum. In the later stage of algorithm implementation, a larger ρ is required to ensure a low residual pheromone concentration on the route, and the global positive feedback needs to be strengthened to improve the running efficiency of the algorithm.

The pheromone-smoothing mechanism employs a real-time adjustment of the pheromone volatility coefficient so that the algorithm can search as many solutions as possible in the initial stage. In addition, the running efficiency to output the global optimum in the later stage is improved, thereby balancing the algorithm's search and utility capacity. The value of ρ in the present work is calculated by Equation (9), where N_c is the current number of iterations and $N_{c\max}$ is the total number of iterations.

$$\rho = \rho_0 + (1 - \rho_0)\frac{N_c}{N_{c\max}} \tag{9}$$

(2) Setting the pheromone concentration of routes within a fixed range of $[\tau_{\min}, \tau_{\max}]$.

A crucial idea of the adaptive ACA is to confine the pheromone concentration on the route within a certain range to avoid large discrepancies between sections and hence to preclude stagnation of the algorithm. The value setting of $\tau_{i,j}(t)$ is shown in Equation (10):

$$\tau_{i,j}(t) = \begin{cases} \tau_{\min}, \tau_{i,j}(t) \le \tau_{\min} \\ \tau_{\max}, \tau_{i,j}(t) \ge \tau_{\max} \end{cases} \tag{10}$$

where τ_{max} is defined as follows:

$$\tau_{max} = \frac{Q}{\rho L_{min}} \quad (11)$$

3. Construction of the Environment Model

3.1. Contributing Factors to Trafficability

3.1.1. Influence of Surface Features on Trafficability

Surface features refer to natural or artificial features on the ground surface, which have varied impacts on trafficability. A vehicle that can drive smoothly on highway will slow down or even get trapped on a sandy road. It is usually difficult to quantify the impacts of surface features on the vehicle speed. To achieve semi-quantitative measurements, we introduced the speed influence coefficient of surface features with reference to the definition of the speed influence coefficient in the literature [31,32]. The coefficient we proposed is the ratio of average driving speed on a certain surface feature to average speed on concrete pavements; the value of the coefficient is within the range of [0, 1], which is used to assign value to the generalized barrier grid map. Table 1 shows the values of the speed influence coefficient of surface feature.

Table 1. Relationship between surface features and speed influence coefficient of surface features.

Level	Surface Feature	Speed Influence Coefficient of Surface Feature
1	Highway	1
2	Bare land	0.6
3	Grassland	0.5
4	Sandy ground	0.3
6	Residential area	0.2
5	Forest	0.1
7	Mire & river	0

3.1.2. Impacts of Terrain on Trafficability

The speed influence coefficient of surface features introduced in the previous section can be better applied to path-planning problems with a smaller scale. However, when it comes to the path-planning problem with a larger scale, for example, when the total length of the path reaches tens of kilometers, the environment modeling will be too complex if only the surface feature description is used. In geography, terrain is a more macroscopic description of ground attributes than surface features. Therefore, this section considers the impact of terrain on trafficability. Terrain is a general term for surface features and geomorphic features. Geomorphic features combined with different surface features comprise different terrains. For instance, deserts comprise the geomorphic feature of plains combined with sandy soil. The speed influence coefficient of terrain is introduced in environment modelling, and the definition is the same as in Section 3.1.1. Table 2 shows the set values of the speed influence coefficient of terrain in this study.

3.2. Simulation Cases of Different Barrier Rates

The vehicle travel time was selected as the major indicator for the algorithm's overall performance. The impact of two speed influence coefficients on the vehicle travelling speed is shown in Equation (12), where $Tra(g_{i,j})$ is the speed influence coefficient corresponding to the grid in row I and column j.

$$v_{i,j} = v_0 \cdot Tra(g_{i,j}) \quad (12)$$

Then, the time that the vehicle travels through the route $i - j$ can be expressed as:

$$t_{i,j} = l_{i,j}/v_{i,j} \quad (13)$$

The improved ACA should adapt to different barriers since the real-world off-road environment is complex. Without a loss of generality, three barrier modes were set respectively on 20 × 20 grid maps. The proportions of the barrier grids, fuzzy grids, and free grids were {15%, 45%, 40%}, {25%, 40%, 35%}, and {35%, 35%, 30%}, respectively. The proportions of these three types of grids were input into Matlab R2019a, and values were assigned randomly to each grid to obtain three generalized barrier grid maps, as shown in Figure 3.

Table 2. Relationship between terrains and speed influence coefficient of terrains.

Level	Terrain	Characteristics	Speed Influence Coefficient of Terrain
1	Plain	Flatland, with an elevation difference less than 50 m.	1
2	Grassland	Relatively flat land, with grass and shrubs as the major surface feature.	0.8
3	Hill	Ground surface without distinct borderlines, and the elevation difference is between 50 and 200 m.	0.5
4	Gobi Desert	Flat and broad ground surface, covered by gravel.	0.3
5	Mountain	Ground surface with large relief and an elevation difference above 200 m.	0.2
6	Residential area	Area with a certain concentration of buildings.	0.2
7	Alpine plateau	Terrain that is a mixture of mountain, plateau, and basin, with an altitude higher than 3000 m.	0.2
8	Coastal island	A narrow corridor that connects ocean and land.	0.2
9	Wooded mountain	Mountains with forest as the main ground object.	0.1
10	Watered paddy fields	Flatland with mild fluctuations and densely distributed water bodies.	0.1

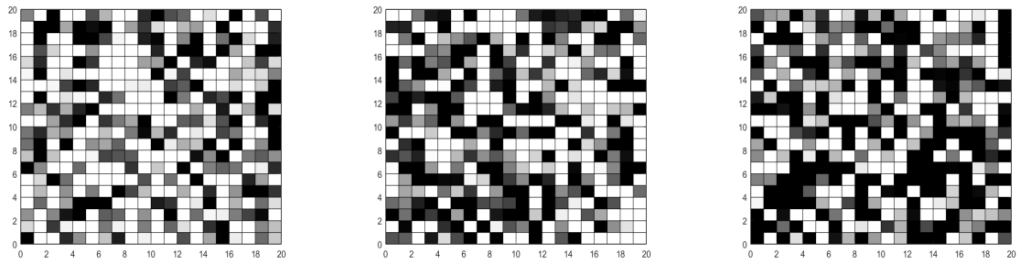

(**a**) (**b**) (**c**)

Figure 3. Generalized barrier grid maps (**a**–**c**).

4. Performance Evaluation of Improved ACA

4.1. Parameter Optimization

Parameters that had considerable impacts on the performance of ACA included the pheromone heuristic factor (α), expectation heuristic factor (β), pheromone volatility factor (ρ), pheromone intensity (Q), and the number of ants (m). In our algorithm, the concept of fuzzy grids was introduced, and therefore it was important to select the trafficability heuristic factor (γ). The selection of parameters substantially affects the convergence and quality of solutions. Up to now, parameter setting has lacked a strict theoretical basis, and no universal methods for parameter configuration are available. Thus, the parameters should be configured as per the requirements of tasks.

(1) Heuristic factors

In the ACA, three heuristic factors interact in a coupling way, and the combination of the three considerably affects the algorithm performance. This section discusses the combination of three heuristic factors.

In the experiment, 100 iterations were set as the condition to terminate the algorithm; while one factor was changed, the other two remained the same to determine the optimal parameters. The default parameter setting was $\{\alpha, \beta, \gamma, \rho, m, Q\} = \{1, 5, 3, 0.4, 50, 20\}$. Within the range of the values, 11 simulation experiments were designed for each heuristic factor; given the randomness of the algorithm, each set of simulation ran 10 times to achieve the average value. Figures 4–6 show the experiment results.

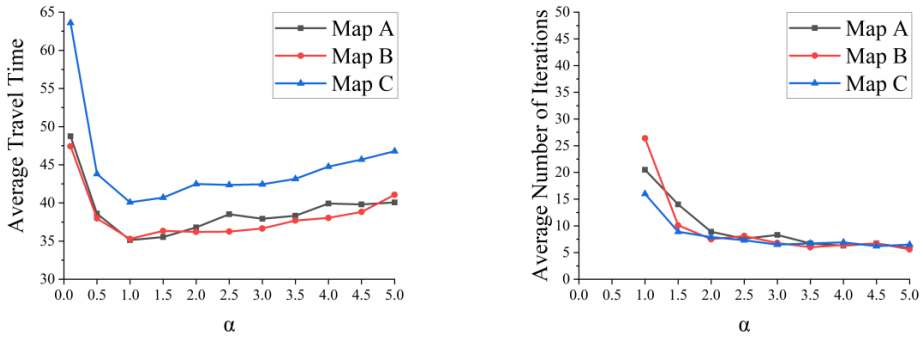

Figure 4. Influence of α on the algorithm's performance. (**a**) The change trend of maneuvering time with α. (**b**) The change trend of iterations time with α.

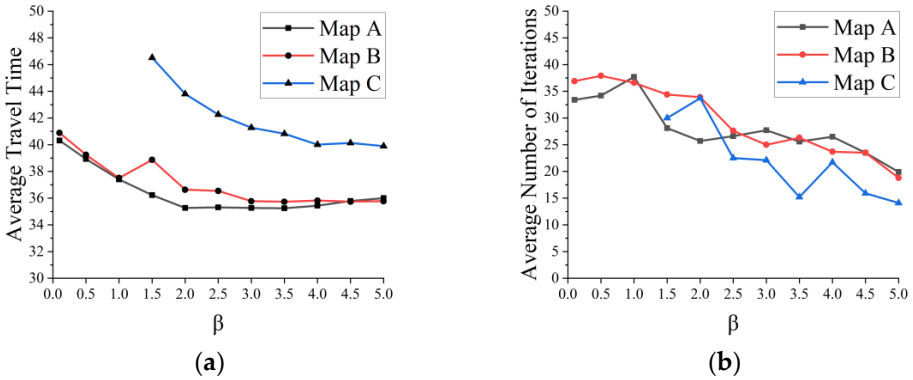

Figure 5. Influence of β on the algorithm's performance. (**a**) The change trend of maneuvering time with β. (**b**) The change trend of iterations time with β.

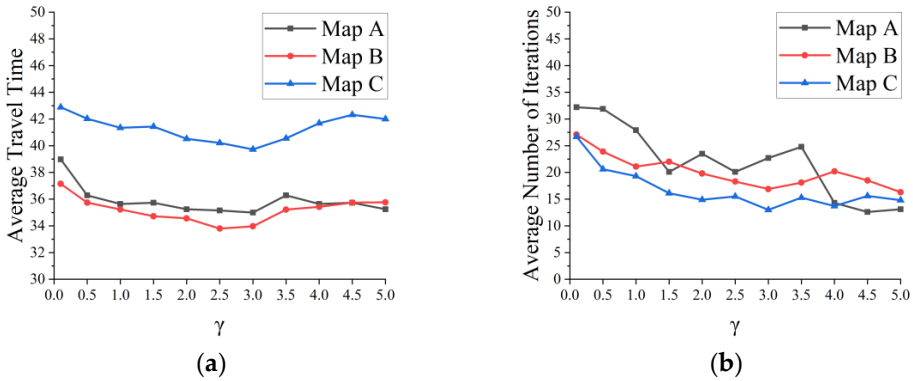

Figure 6. Influence of γ on the algorithm's performance. (**a**) The change trend of maneuvering time with γ. (**b**) The change trend of iterations time with γ.

As Figure 4a shows, on the three maps, when α increased from 0 to 1, the average traveling time dropped considerably; when α continued to increase, the average traveling time presented a trend of mild growth. As Figure 4b shows, when α was between 0.1 and 0.5, the algorithm failed to converge after 100 iterations. This was because when the value of α was small, the guiding effect of pheromone on the ant's foraging was weak, and the ant could not gain heuristic experience from the former ants; as a result, the algorithm diverged. The average traveling time in Figure 4a is the average value for the shortest route after 50 iterations. As α continued to grow from 1.0 to 1.5, the average number of iterations significantly declined before leveling off. With the average traveling time and the average number of iterations taken into account, the pheromone heuristic factor was set at 1; that is, $\alpha = 1$.

As Figure 5a shows, as β grew, the average traveling time on the three maps declined before leveling off. On map C, errors were reported in the algorithm when the value of β was small. This was because map C had a high barrier rate and complex environmental information, and the ant was unable to find a way with a small expectation heuristic factor. As Figure 5b shows, the average number of iterations presented a linear declining trend with the increase in β. With the average traveling time and average number of iterations considered, the expectation heuristic factor was set at 4; that is, $\beta = 4$.

As Figure 6a shows, when $\gamma < 3$, as the value of γ grew, the average traveling time on the maps presented a trend of mild decline; when $\gamma > 3$, the average traveling time slightly rose as the value of γ increased. As Figure 6b shows, with the increase in γ, the average number of iterations declined linearly, but the decline was not as sharp as that in Figure 5b. With the average traveling time and average number of iterations considered, the trafficability heuristic factor was set at 3; that is, $\gamma = 3$.

(2) Pheromone volatility coefficient

The major improvement in the ACA in this study was the pheromone concentration of routes; therefore, the value of the pheromone volatility coefficient is discussed as follows. Eleven simulated experiments were designed for the value range of the coefficient, and the other parameters remained the same as in the default setting. The experimental method was the same as above, and the results are shown in Figure 7.

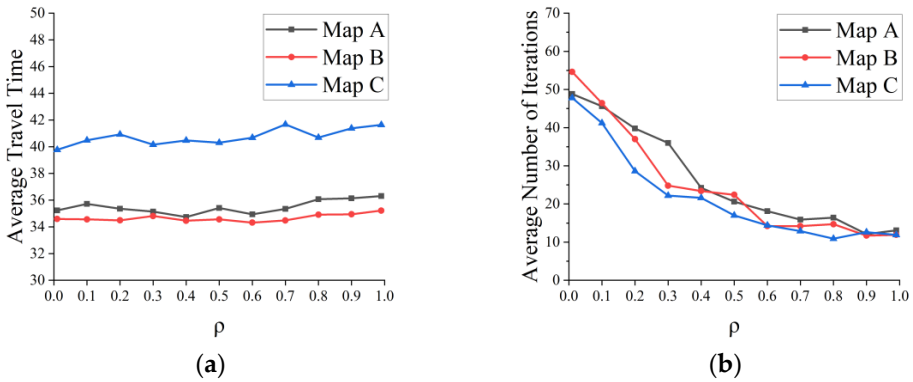

Figure 7. Influence of ρ on the algorithm's performance. (**a**) The change trend of maneuvering time with ρ. (**b**) The change trend of iterations time with ρ.

As Figure 7a shows, with the increase in ρ, the average traveling time on different maps showed no tangible changes. In a conventional ACA, ρ is a key factor that affects the algorithm's performance. Figure 7a proves that our improved algorithm was more robust than the conventional one. As Figure 7b shows, the average number of iterations decreased as ρ increased, and when $\rho > 0.4$, the decline slowed. Prior experience shows that the value of ρ should not be extremely large or small. Therefore, the pheromone volatility coefficient was set at 0.4; that is, $\rho = 0.4$.

(3) Number of ants

The value of m was determined by simulation experiments. The average traveling time and average number of iterations were calculated with the number of ants set at 5, 10, 25, 50, 100, 150, and 200. Figure 8 shows the experiment results.

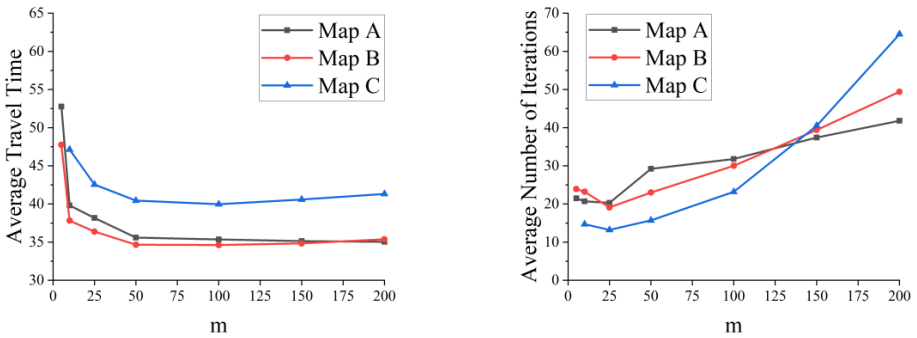

(**a**) (**b**)

Figure 8. Influence of m on the algorithm's performance. (**a**) The change trend of maneuvering time with m. (**b**) The change trend of iterations time with m.

As Figure 8a shows, when $m < 50$, the average traveling time on different maps significantly dropped with the increase in m; on map C, the algorithm reported an error at a small value of m. This was because map C had a high barrier rate and complex environments, making it difficult for the ants to find a route if the colony is too small. As m continued to grow, the average traveling time became stable. As Figure 8b shows, the number of iterations slightly declined at a small colony (when $m < 25$) but grew quickly as m grew, and the algorithm showed poor convergence performance. Therefore, the number of ants was set at 50 in the present work; that is, $m = 50$.

(4) Pheromone intensity

The influence of pheromone intensity on the algorithm's performance relies on the configuration of the heuristic factor and the pheromone volatility factor; therefore, after the optimal values of these two parameters were determined via simulations, the value of Q was set at 10 ($Q = 10$) to keep the value of Q aligned with the pheromone concentration.

4.2. Performance Evaluation

4.2.1. Construction of Path-Planning Maps

To validate our improved algorithm, path-planning simulations were performed on two regions (400 m × 400 m) on high-resolution remote-sensing images of Beishan Town and Xingsha Street (28°24′ N, 113°00′ E; 28°15′ N, 113°06′ E) in Changsha, Hunan. Figures 9a and 10a show the satellite remote-sensing images of the two study cases. The images were converted to 20 × 20 grids, and hence 20 × 20 grid maps were generated. Figures 9b and 10b show the grid maps without consideration of trafficability; Figures 9c and 10c show the generalized barrier grid maps after weights were assigned to the grids based on the speed influence coefficient of surface features.

4.2.2. Simulation Experiments

On the generalized barrier grid maps for the two selected areas, we conducted path-planning simulation experiments using the traditional ACA that does not consider trafficability (T-ACA-NT), the traditional ACA that considers trafficability (T-ACA-T), and our improved ACA that considers trafficability (I-ACA-T). The simulation results are shown in Figures 11 and 12. Given the randomness of the experiments, each set of simulations ran 10 times to obtain the average value, and the results are shown in Tables 3 and 4.

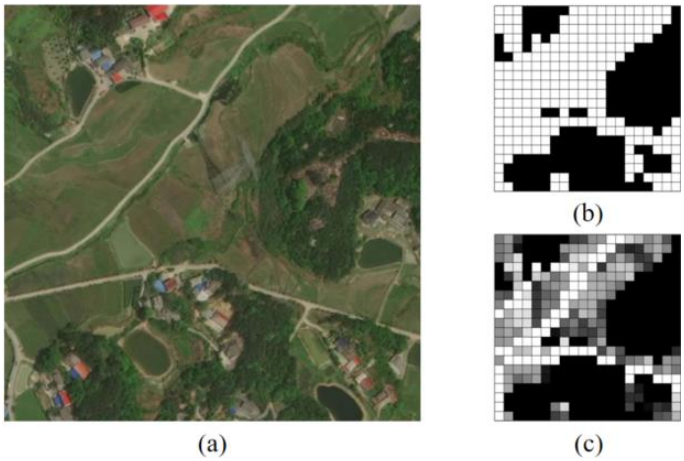

Figure 9. Maps of Beishan Town (selected area). (**a**) Original remote sensing image map. (**b**) 01 map. (**c**) Generalized obstacle grid map.

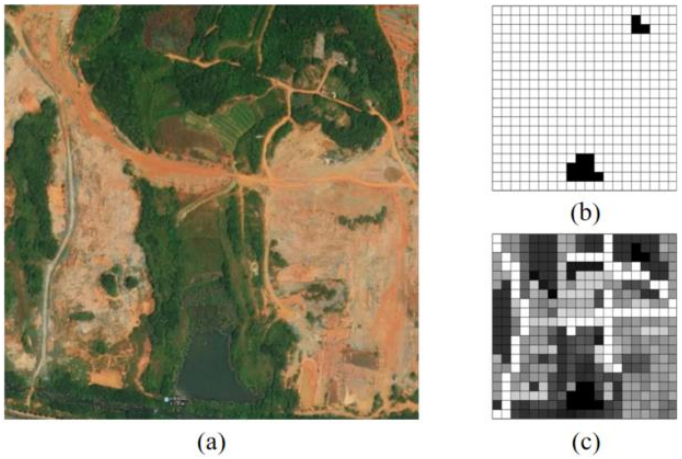

Figure 10. Maps of Xingsha Street (selected area). (**a**) Original remote sensing image map. (**b**) 01 map. (**c**) Generalized obstacle grid map.

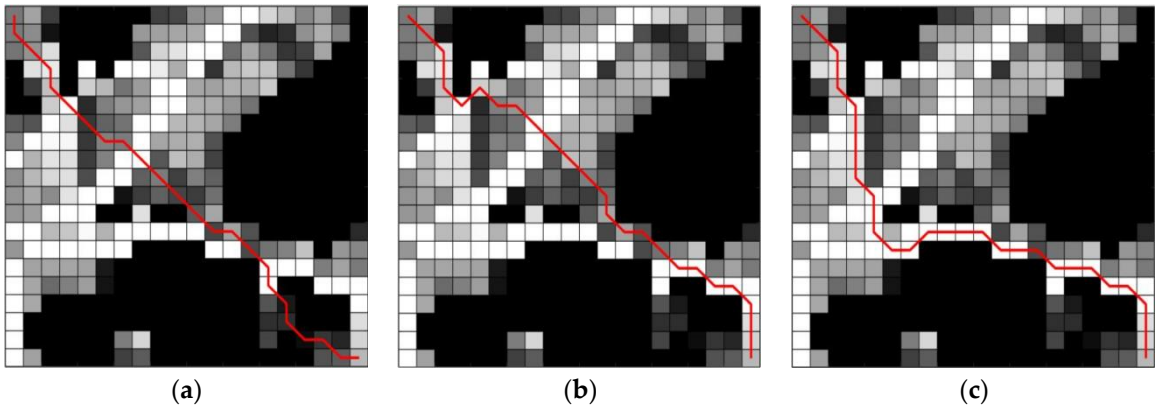

Figure 11. Path-planning diagram in Beishan Town (selected region). (**a**) Path planning diagram of T-ACA-NT. (**b**) Path planning diagram of T-ACA-T. (**c**) Path planning diagram of I-ACA-T (our algorithm).

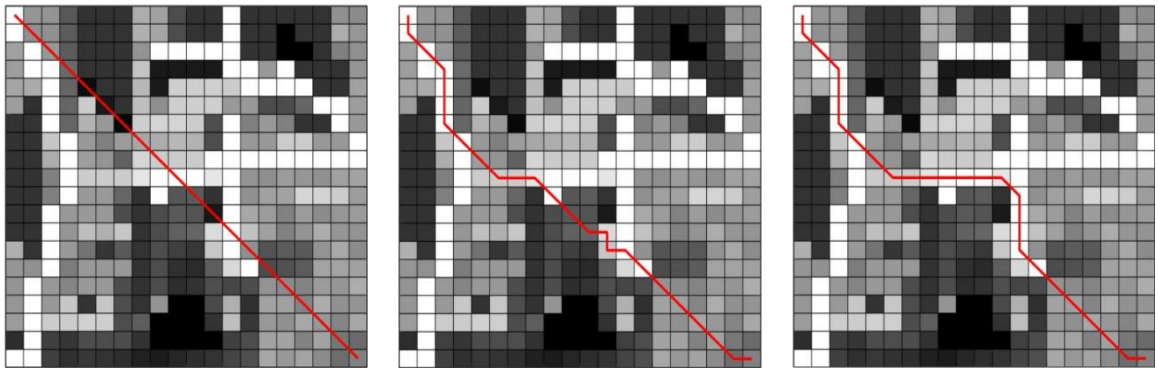

(**a**) (**b**) (**c**)

Figure 12. Path-planning diagram of Xingsha Street (selected region). (**a**) Path planning diagram of T-ACA-NT. (**b**) Path planning diagram of T-ACA-T. (**c**) Path planning diagram of I-ACA-T (our algorithm).

Table 3. Path-planning simulation results in Beishan Town (selected region).

	Total Length of Route (m)	Traveling Time (s)	Number of Iterations
T-ACA-NT	584.26	106.41	46.4
T-ACA-T	719.41	88.40	36.7
I-ACA-T (our algorithm)	714.64	87.81	20.3

Table 4. Path-planning simulation results in Xingsha Street (selected region).

	Total Length of Route (m)	Traveling Time (s)	Number of Iterations
T-ACA-NT	540.92	99.39	42.5
T-ACA-T	635.21	77.32	21.6
I-ACA-T (our algorithm)	643.70	77.28	14.1

Analyses of Figures 11 and 12 and Tables 3 and 4 revealed the following findings:

(1) In terms of convergence speed, the T-ACA-T reduced the iterations by 20.91% and 49.18% in comparison with T-ACA-NT; our improved ACA that considers trafficability (I-ACA-T) reduced the number of iterations by 56.25% and 66.82% in comparison with T-ACA-NT. To sum up, our improved ACA significantly improved the convergence and computing efficiency.

(2) In terms of the quality of solutions, T-ACA-T reduced the traveling time by 16.93% and 22.21% despite a slight increase in the route length; our I-ACA-T reduced the traveling time by 17.48% and 22.25%. Our improved ACA showed no significant improvement on the traveling time in comparison with T-ACA-T. Nonetheless, as Figures 11b,c and 12b,c show, our algorithm was more likely to find the global optimum, whereas T-ACA-T was susceptible to the local optimum.

(3) In terms of the stability of path planning, our algorithm achieved quick convergence on two maps of different barrier rates; furthermore, variance analysis showed that the algebraic difference in convergence between the different cases had no statistical significance. Thus, our improved algorithm had strong robustness.

5. Multilevel Adaptive Path-Planning Model Based on Improved ACA

The traveling environment of off-road vehicles is a mixture of paved and unpaved roads, and hence path planning that relies merely on road network information or off-road environments is hardly feasible in real-world scenarios. In addition, the length of off-road

vehicles ranges from several miles to several hundred miles; therefore, it is challenging to balance precision and breadth in path planning. In this study, a multilevel adaptive path-planning model was proposed to meet the requirements for vehicle trafficability, off-road trafficability, rough planning, and accurate planning.

5.1. Primary Path Planning

When the area of the off-road environment ranges from several hundred to several hundred thousand square kilometers, high-precision path planning will require a huge investment of time and computing resources. Thus, instead of high-precision modeling, a rough and macroscopic description based on semi-quantitative empirical parameters is more applicable. The generalized barrier grid map was constructed based on the correlation between the terrain and speed influence factor, and the length of the grid edge was set at 10 km.

A 100 km × 100 km square area in the Midwest of Henan Province, China (33°38′32″ N–34°32′21″ N, 112°34′48″ E–113°39′36″ E) was used to simulate the off-road environment. Figure 13 shows the remote sensing image of the selected simulated combat area. The area studied was at Pingdingshan City and Luoyang City, along the borders between Funiu Range and the North China Plain. This area was a representative sample for path planning since this area has various surface features.

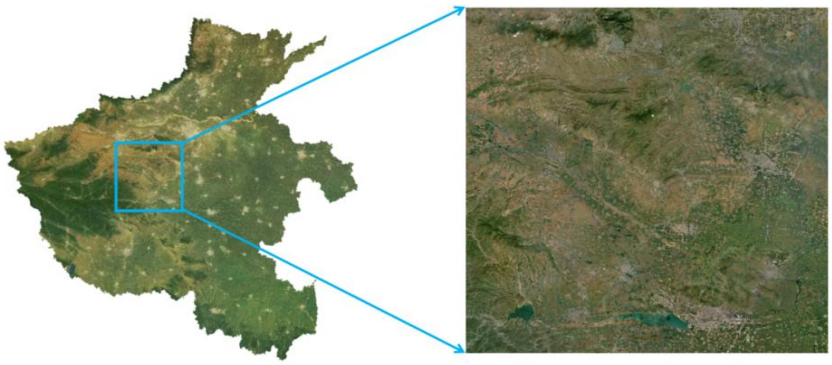

Figure 13. Remote-sensing image of the off-road environment for simulation (primary).

The remote-sensing image of the selected area for simulation was converted into a grid map; each grid covered an area of 10 km × 10 km. The remote-sensing image-classification method was used to classify the grids, and the area-dominance method was used to ensure that each grid had only one type of terrain; that is, the dominating type of terrain was considered as the terrain type of the whole grid. In this way, a 10 × 10 generalized barrier grid map was generated, where the grid at the first line and first column was set as the starting point, and the grid at the 10th line and 10th column was set as the destination. Figure 14 shows the planned path.

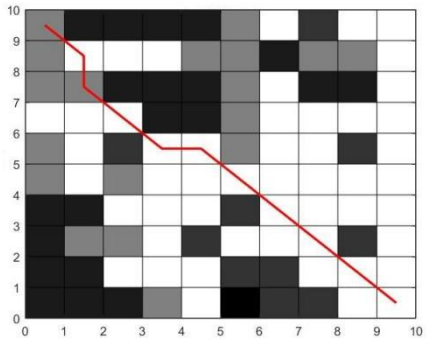

Figure 14. Planned route obtained in primary path planning.

5.2. Secondary Path Planning

When the area of the off-road environment is less than a hundred square kilometers, the modeling precision will to some extent affect the quality of path-planning solutions. A relatively small area is not likely to have evident terrain changes; therefore, a constructed grid map will present a monotonous pattern of terrain if this terrain is used as the basis of modeling. To precisely describe the off-road area, we considered the vehicle travel time as a function of the surface-feature attribute and generalized the grid maps based on the relationship between the surface-feature attribute and speed influence coefficient. The length of the grid edge was set at 0.5 km.

As Figure 14 shows, the terrain in the grid at the third line and second column was hills; in the primary path planning, this grid was on a planned path. This grid was set as the studied object in secondary path planning, and Figure 15 shows the remote-sensing image.

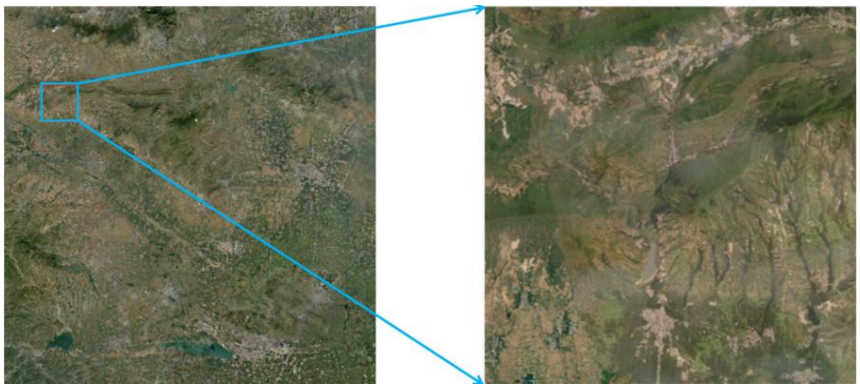

Figure 15. Remote-sensing image of the simulated off-road area (secondary).

The selected area was converted into a grid map, with the size of the grids set at 0.5 km × 0.5 km. The remote-sensing image-classification algorithm was used to classify the grids, and the area dominance method was used to identify the ground object attribute of each grid. With these measures, a 20 × 20 generalized obstacle grid map was generated. The grid at the first line and 11th column was set at the starting point, and the grid at the 20th line and 20th column was set as the destination. Figure 16 shows the planned path.

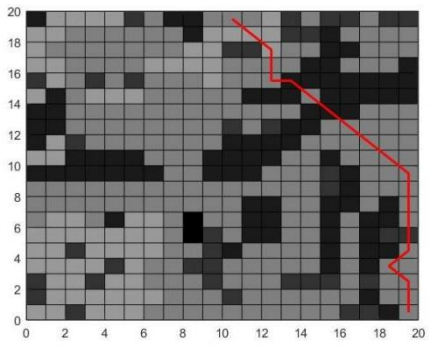

Figure 16. Diagram of the route achieved in secondary path planning.

5.3. Tertiary Path Planning

After secondary path planning, the size of the grid was still at the level of several hundred meters, far larger than the length of off-road vehicles, which is just several meters. Therefore, secondary path planning could not satisfy the needs and further classification of the grid was required. The vehicle trafficability was set as the function of the ground object attributes; generalized grid maps were constructed based on the relationship between the

ground object attribute and speed influence coefficient, and the edge of the grid was set at 25 m.

In tertiary path planning, the grid size is close to the size of the vehicle; therefore, instead of simply taking the vehicle as the mass point, the impact of the vehicle size on trafficability should be considered. In the transfer strategy of the algorithm, both fuzzy grids and free grids were considered as trafficable grids, whereas obstacle grids were not considered trafficable. However, the impact on the trafficability of the diagonal line of neighboring obstacle grids was not considered, as shown in Figure 17a. Therefore, in the environment modeling of tertiary path planning, the concept of obstacle inflation was introduced, which was intended to expand the range of obstacles. Specifically, the speed influence coefficient of grids adjacent to an obstacle grid was halved, as shown in Figure 17b. This increased the safety factor of the planned path.

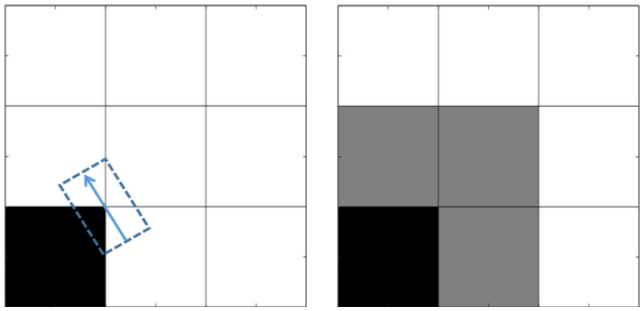

Figure 17. Rules for obstacle inflation. (**a**) Collision may occur before obstacle expansion treatment. (**b**) Environmental model after obstacle expansion treatment.

As Figure 16 shows, the surface feature of the grid at the 10th line and 19th column in the off-road area was grassland, and in the primary path planning, this grid was on the planned route. This grid was the study object in the tertiary path planning, and Figure 18 shows the corresponding remote-sensing image.

Figure 18. Remote-sensing image of the simulated off-road environment (tertiary path planning).

The selected area was converted into a grid map, with the size of grids set at 25 m × 25 m. The remote-sensing image-classification algorithm was used to classify the grids, and the area dominance method was used to identify the ground object attribute of each grid, but this identification approach differed from that in the primary and secondary path planning. The speed influence coefficient of highways was 1, that is, the highway had the largest probability to be chosen in the path planning of optimal trafficability. In the tertiary planning, if there was a highway in a grid, then the attribute of this grid was defined as highway, regardless of how much area that the highway took up in the grid. With these measures, a 20 × 20 generalized obstacle grid map was generated. In the process

of secondary path planning, the planned path entered from the upper-left corner of the grid and passed through the lower right corner; therefore, the grid at the 1st line and 1st column was set as the starting point, and the grid at the 20th line and 20th column was set as the destination. Figure 19 shows the planned route.

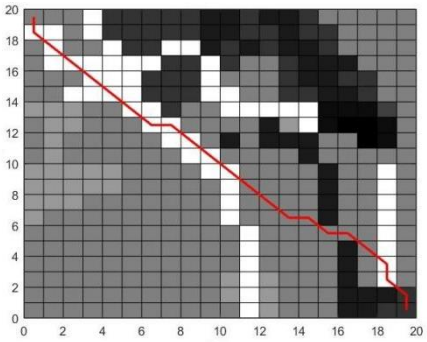

Figure 19. The route achieved by tertiary path planning.

5.4. Advantages of Multilevel Adaptive Path Planning

The multilevel adaptive path planning scheme consisted of the primary, secondary, and tertiary path-planning algorithms. As the applied area differed, the environment modelling and path planning in these algorithms varied as well. Figure 20 shows the meaning of multi-level adaptive path planning.

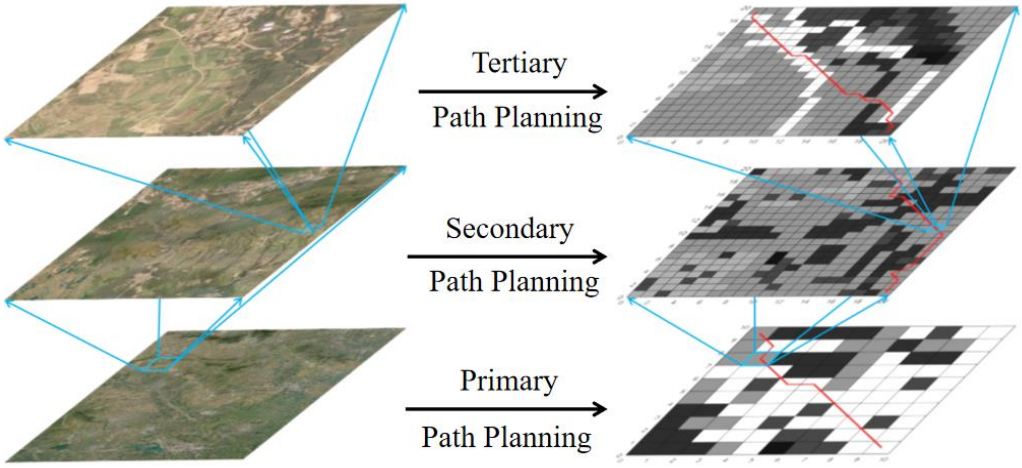

Figure 20. Path planning by the multilevel adaptive model.

The multilevel adaptive path-planning model had the following advantages.

(1) The model reduced computing overheads. For a given area to be studied, the computing overhead was proportional to the computing accuracy. Nearly unbearable computing overheads are required to plan a path with a meter-level accuracy in an off-road environment with a magnitude of several hundred meters by traditional methods. The multilevel adaptive method, however, divided the path planning task into three steps, which dispensed with the need for rigorous environment modeling and hence balanced computing accuracy with computing difficulty.

(2) The model was applicable to off-road areas of different sizes. In the multilevel adaptive level, the primary and secondary path-planning algorithms did not consider the problem of road networks, but in the tertiary planning, the highway information was considered. Therefore, paved roads were prioritized in path planning to achieve universality for different off-road environments.

6. Conclusions

In this study, the traditional ant colony algorithm was improved for path planning in off-road environments. Simulation experiments were designed to optimize the key parameters in the algorithm. The selected areas in the remote-sensing images of Changsha in Hunan Province, China, were converted into grid maps to validate the performance of the algorithm. Three algorithms—a traditional ACA that does not consider trafficability, a traditional ACA that considers trafficability, and an improved ACA that considers trafficability—were used for the path planning. The experiments showed that the improved algorithm could achieve a higher computing efficiency, solutions of a better quality, and a higher stability. Thus, based on the improved ACA, a multilevel adaptive path-planning model was proposed. Consisting of primary, secondary, and tertiary path planning, the model could plan a path in an off-road area of several hundred thousand square kilometers, which balances computing accuracy and breadth while reducing the computing overhead.

Author Contributions: Conceptualization, X.S. and J.G.; methodology, J.G.; software, X.S.; validation, X.S. and J.G.; formal analysis, X.S.; investigation, X.S.; resources, X.S.; data curation, J.G.; writing—original draft preparation, X.S.; writing—review and editing, J.G.; visualization, X.S.; supervision, X.S.; project administration, J.G.; funding acquisition, J.G. All authors have read and agreed to the published version of the manuscript.

Funding: This research received no external funding.

Institutional Review Board Statement: Not applicable.

Informed Consent Statement: Not applicable.

Data Availability Statement: The data that support the findings of this study are available from the corresponding author upon request.

Conflicts of Interest: The authors declare no conflict of interest.

References

1. Dekker, R.; Koster, R.; Kim, K. Maritime and container logistics. *Flex. Serv. Manuf. J.* **2017**, *29*, 1–3. [CrossRef]
2. Hao, L.; Ma, G.; Dong, J. Path Planning Method of Anti-Collision for the Operation Road of Port Cargo Handling Robot. *J. Coast. Res.* **2020**, *103*, 892–895. [CrossRef]
3. Ferrell, W.; Ellis, K.; Kaminsky, P.R. Horizontal collaboration: Opportunities for improved logistics planning. *Int. J. Prod. Res.* **2019**, *58*, 4267–4284. [CrossRef]
4. HyeokSoo, L.; Jongpil, J. Mobile Robot Path Optimization Technique Based on Reinforcement Learning Algorithm in Warehouse Environment. *Appl. Sci.* **2021**, *11*, 1209.
5. Velez-Lopez, G.C.; Vazquez-Leal, H.; Hernandez-Martinez, L.; Sarmiento-Reyes, A.; Diaz-Arango, G.; Huerta-Chua, J.; Rico-Aniles, H.D.; Jimenez-Fernandez, V.M. A Novel Collision-Free Homotopy Path Planning for Planar Robotic Arms. *Sensors* **2022**, *22*, 4022. [CrossRef]
6. Mohseni, A.; Duchaine, V.; Wong, T. Experimental study of path planning problem using EMCOA for a holonomic mobile robot. *J. Syst. Eng. Electron.* **2021**, *32*, 1450–1462.
7. Phone, T.K.; Anh, V.L.; Prabakaran, V.; Mohan, R.E.; Theint, T.T.; Nguyen, H.K.; Phan, V.D. Energy-Efficient Path Planning of Reconfigurable Robots in Complex Environments. *IEEE Trans. Robot.* **2022**, *38*, 2481–2494.
8. Sick, A.G. Telegrams for Operating/Configuring the LMS2XX Laser Measurement Systems. *J. Firmware Version* **2003**, *2*, X1.
9. Brand, M.; Masuda, M.; Wehner, N.; Yu, X.-H. Ant colony optimization algorithm for robot path planning. In Proceedings of the 2010 International Conference on Computer Design and Applications, Qinhuangdao, China, 25–27 June 2010; Volume 3, pp. V3-436–V3-440.
10. Zheng, W.; Guan, W.; Cheng, Y. Robot path planning based on TGSA and three-order bezier curve. *Rev. D'intell. Artif.* **2018**, *32*, 41.
11. Song, B.; Park, K.; Kim, J. Persistent UAV delivery logistics: MILP formulation and efficient heuristic. *Comput. Ind. Eng.* **2018**, *120*, 418–428. [CrossRef]
12. Alejandro, P.C.; Daniel, R.; Alejandro, P.; Enrique, F.B. A review of artificial intelligence applied to path planning in UAV swarms. *Neural Comput. Appl.* **2022**, *34*, 153–170.
13. Vundurthy, B.; Sridharan, K. Multiagent Gathering with Collision Avoidance and a Minimax Distance Criterion—Efficient Algorithms and Hardware Realization. *IEEE Trans. Ind. Inform.* **2018**, *15*, 699–709. [CrossRef]
14. Ropero, F.; Muñoz, P.; María, D. TERRA: A path planning algorithm for cooperative UGV-UAV exploration. *Eng. Appl. Artif. Intell.* **2019**, *78*, 260–272. [CrossRef]

15. Pritam, K.; Kashish, D.; William, J.B.; Animesh, C. Vision-Based Guidance for Tracking Dynamic Objects. In Proceedings of the 2021 International Conference on Unmanned Aircraft Systems (ICUAS), Athens, Greece, 15–18 June 2021.
16. Kashish, D.; Abhishek, K.; Animesh, C. Collision Avoidance and Rendezvous of Quadric Surfaces Moving on Planar Environments. In Proceedings of the 2021 60th IEEE Conference on Decision and Control, Austin, TX, USA, 13–17 December 2021.
17. Kanhaiya, L.C.; Debasish, G. Path planning in dynamic environments with deforming obstacles using collision cones. In Proceedings of the 2017 Indian Control Conference, Guwahati, India, 4–6 January 2017.
18. Fu, J.; Lv, T.; Li, B. Underwater Submarine Path Planning Based on Artificial Potential Field Ant Colony Algorithm and Velocity Obstacle Method. *Sensors* **2022**, *22*, 3652. [CrossRef]
19. Dorigo, M.; Maniezzo, V.; Colorni, A. *The Ant System: An Autocatalytic Optimizing Process*; CiteSeer; Dipartimento Di Elet-tronica, Politecnico Di Milano: Milan, Italy, 1991.
20. Ezhilarasi, T.P.; Rekha, K.S. Improved fuzzy ant colony optimization to recommend cultivation in Tamil Nadu, India. *Acta Geophys.* **2022**, 1–15. [CrossRef]
21. Chao, N. Path Planning Based on Improved Ant Colony Algorithm. Ph.D. Thesis, Harbin University of Science and Technology, Harbin, China, 2019.
22. Keonyup, C.; Minchae, L.; Myoungho, S. Local path planning for off-road autonomous driving with avoidance of static obstacles. *IEEE Trans. Intell. Transp. Syst.* **2012**, *13*, 1599–1616.
23. Chen, J.; Jiang, W.; Zhao, P.; Hu, J. A path planning method of anti-jamming ability improvement for autonomous vehicle navigating in off-road environments. *Ind. Robot. Int. J.* **2017**, *44*, 406–415. [CrossRef]
24. Wang, H.; Zhang, H.; Wang, K.; Zhang, C.; Yin, C.; Kang, X. Off-road path planning based on improved ant colony algorithm. *Wirel. Pers. Commun.* **2018**, *102*, 1705–1721. [CrossRef]
25. Hu, J.; Hu, Y.; Liu, K.; Wang, W.; Chen, H. Off-road Terrain Path Planning for Differential Steering Vehicles Based on Artificial Potential Field Gradient. In Proceedings of the IEEE Intelligent Transportation Systems Conference (IEEE-ITSC), Auckland, New Zealand, 27–30 October 2019.
26. Yonghoon, J.; Tanaka, Y.; Tamura, Y.; Kimura, M.; Umemura, A.; Kaneshima, Y.; Murakami, H.; Yamashita, A.; Asama, H. Adaptive Motion Planning Based on Vehicle Characteristics and Regulations for Off-Road UGVs. *IEEE Trans. Ind. Inform.* **2019**, *15*, 599–611.
27. Yang, L.; Gong, J.; Xiong, G.; Yang, T.; Wu, M.; Zhang, S. Unmanned Vehicle Path Planning for Unknown Off-road Environments with Sparse Waypoints. In Proceedings of the IEEE Intelligent Transportation Systems Conference, Auckland, New Zealand, 27–30 October 2019.
28. Chen, J.; Zhen, H.; Zissimos, P.M.; David, G.; Paramsothy, J.; Yan, F.; Monica, M. R2-RRT*: Reliability-Based Robust Mission Planning of Off-Road Autonomous Ground Vehicle Under Uncertain Terrain Environment. *IEEE Trans. Autom. Sci. Eng.* **2022**, *19*, 1030–1046.
29. Goodin, C.; Doude, M.; Hudson, C.R.; Caruth, D.W. Enabling Off-road Autonomous Navigation-simulation of LIDAR in Dense Vegetation. *Electronics* **2018**, *7*, 154. [CrossRef]
30. Hong, Z.; Sun, P.; Tong, X.; Pan, H. Improved A-Star Algorithm for Long-Distance Off-Road Path Planning Using Terrain Data Map. *ISPRS Int. J. Geo. Inf.* **2021**, *10*, 785. [CrossRef]
31. Zhao, M. Track Planning of Ground Unmanned Platform in Cross-Country Environment. Ph.D. Thesis, The North China University of Technology, Beijing, China, 2021.
32. Sun, Y. Global Path Planning and Trajectory Tracking of Unmanned Wheeled Vehicles on Terrains. Ph.D. Thesis, Jilin University, Changchun, China, 2020.